Cell. Mol. Life Sci. (2010) 67:2825–2838
DOI 10.1007/s00018-010-0363-1

Cellular and Molecular Life Sciences

RESEARCH ARTICLE

# The structural intolerance of the PrP α-fold for polar substitution of the helix-3 methionines

**Silvia Lisa · Massimiliano Meli · Gema Cabello · Ruth Gabizon · Giorgio Colombo · María Gasset**

Received: 21 February 2010 / Revised: 17 March 2010 / Accepted: 19 March 2010 / Published online: 9 May 2010


**Abstract** The conversion of the cellular prion protein ($PrP^C$) into its disease-associated form ($PrP^{Sc}$) involves a major conformational change and the accumulation of sulfoxidized methionines. Computational and synthetic approaches have shown that this change in the polarity of M206 and M213 impacts the C-terminal domain native α-fold allowing the flexibility required for the structural conversion. To test the effect in the full-length molecule with site-specificity, we have generated M-to-S mutations. Molecular dynamics simulations show that the replacement indeed perturbs the native state. When this mutation is placed at the conserved methionines of HaPrP(23–231), only substitutions at the Helix-3 impair the α-fold, stabilizing a non-native state with perturbed secondary structure, loss of native tertiary contacts, increased surface hydrophobicity, reduced thermal stability and an enhanced tendency to aggregate into protofibrillar polymers. Our work supports that M206 and M213 function as α-fold gatekeepers and suggests that their redox state regulate misfolding routes.

**Keywords** Protein conformational switches · Methionine oxidation · Prion protein conversion · Amyloids

**Abbreviations**

| | |
|---|---|
| $PrP^C$ | Cellular prion protein |
| $PrP^{Sc}$ | Disease-related form of PrP |
| HuPrP(125–229) | Polypeptide chain representing the globular domain of the human PrP |
| HaPrP(23–231) | Polypeptide chain representing the mature chain of the hamster PrP |
| MD | Molecular dynamics |
| RWISP | Root weighted square inner product |
| CP | Communication propensity |
| CD | Circular dichroism |
| DLS | Dynamic light scattering |
| $R_h$ | Hydrodynamic radius |
| ThT | Thioflavin T |
| AFM | Atomic force microscopy |

## Introduction

Prions are infectious proteins that use a conformational code for self-perpetuation. In mammals, prions causing transmissible neurodegenerative disorders are composed mainly of $PrP^{Sc}$, an altered form of the cellular prion protein ($PrP^C$) [1, 2]. The long-standing hypothesis of prion biology is that the distinct biological and physicochemical properties separating $PrP^C$ and $PrP^{Sc}$ relate only to the conformational differences of the C-terminal domain, which adopts a major globular α-fold in $PrP^C$ and displays a high content of β-sheet structure in $PrP^{Sc}$ [3–11]. However, the populations of $PrP^C$ and $PrP^{Sc}$ also differ in the

S. Lisa and M. Meli contributed equally to this work.

S. Lisa · G. Cabello · M. Gasset (✉)
Instto Química-Física "Rocasolano", CSIC,
Serrano 119, 28006 Madrid, Spain
e-mail: mgasset@iqfr.csic.es

M. Meli · G. Colombo
Istituto di Chimica del Riconoscimento Molecolare,
Consiglio Nazionale delle Ricerche, Via Mario Bianco 9,
20131 Milan, Italy

R. Gabizon
Department of Neurology, The Agnes Ginges Center for Human Neurogenetics, Hadassah University Hospital,
91120 Jerusalem, Israel

redox state the methionines of Helix-3, suggesting a possible role for these residues in facilitating the structural change [12–15].

The chain reorganization accompanying the conversion of $PrP^{C}$ to $PrP^{Sc}$ proceeds through a complex pathway involving the obligatory initial destabilization of the $PrP^{C}$ α-fold for its subsequent refolding and assembly into $PrP^{Sc}$ [1, 9, 16–19]. Similarly to tau, the hyperphosphorylation of which impairs function and provokes accumulation, sulfoxidation of PrP methionines could also regulate the folding repertoire through the reorganization of intra- and intermolecular bonds [9, 20–22]. As opposed to the enzymatic nature of phosphorylation, methionine sulfoxidation is a chemical modification that takes place in response to oxidative insults and lacks sequence specificity [23–26]. The oxidation product, a mixture of *R,S*-sulfoxide isomers, is reversed by the action of the isomer-specific methionine sulfoxide reductases (MrsA and MsrB), both of which are impaired on ageing [23, 24].

The theoretical analysis of the structural and dynamic impact of the sulfoxidation of any of the Helix-3 methionines conserved within all mammalian species studied has suggested its potential as a destabilizing switch [14]. These modifications alter the stability of the α-fold by disrupting the network of inter-residue interactions responsible for its stability. This destabilization in turn determines a decrease in the internal dynamic coordination of the native state, favoring the transition to alternative conformational states. Synthetic approaches focused on this region of the protein have shown that site-specific substitution of these Met residues with either the more hydrophobic norleucine or the highly hydrophilic methoxinine does in fact modulate the conformation of the chain and its aggregation behavior [15]. However, $PrP^{Sc}$ formation requires a larger polypeptide chain than that accessible to conventional solid-phase synthesis and its high number of Met residues precludes the control in the residue number and position of the covalent modification using chemical oxidative approaches [4, 23–27].

To test the theoretical predictions on experimental grounds, we have used the full-length PrP, the mature chain without signal peptides, and employed mutagenesis to confer site-specificity in the changes [4, 28, 29]. We chose Ser to replace Met since, while it is shorter than Met and chemically different from the sulfoxidized version of Met (MetO), Ser retains the helical propensity and polarity of the MetO [29]. The other possibility previously used for such substitution would be Gln. However, while this amino acid also retains some helical propensity and reproduces the length of the chain, its polarity arises from an amide bond, not only oxygen [30]. In addition, Gln is over-represented in prion-forming sequences, therefore possibly leading to other effects [31]. This strategy, based on providing a property of the covalent modification by mutagenesis (here, the polarity of MetO mimicked with Ser replacement) has been previously used in mimicking Ser/Thr phosphorylation by Asp substitution in the study of the independent and site effects in proteins containing multiple modification sites [22].

Using wt HaPrP(23–231) as the template for mutagenesis, biophysical studies show that the M-to-S replacement of any of the conserved methionines of Helix-3, singly or in combination, prevents the formation of the α-fold and stabilizes a non-native intermediate state with an increased tendency for aggregation and amyloid formation tendency.

## Materials and methods

### Molecular dynamics

Molecular dynamics (MD) simulations were performed using the 3D structure of HuPrP(125–229) (PDB entry 1QLZ) as a starting point essentially as described [14]. M-to-S mutations were generated at the desired positions by side chain replacement using the MUTATE command of the WHATIF package [14, 32]. Oxidation variants were generated by replacing the sulfur atoms of M206, M213, or both by an (*S*)-sulfoxide group as reported previously [14]. For each system, two independent long-time scale all-atom MD simulations were performed in explicit water at 310 K. Each 100-ns simulation was run independently using different sets of initial velocities as described previously [14]. The two simulations for each system were combined and analyzed in terms of the dynamic subspace spanned and the internal dynamics using different approaches to identify structural and dynamic similarities/differences introduced in the α-fold. Structural comparison of HuPrP and HaPrP α-folds was performed using the overlapped region of their 3D structures (PDB entries 1QLZ and 1B10) [14, 33]. The similarities/differences in the environments of M206 or M213 in the two species were evaluated by calculating all the residues in non-bonded contact with either of them using the Maestro Software package from Schrödinger Inc.

### Mutation, production, and folding of the HaPrP(23–231) chains

HaPrP(23–231) chains were produced, purified, and refolded into the α-form from their pET11a constructs using oxidized glutathione for disulfide bond formation and including 2 mM Met in the refolding buffers [27, 34]. The protein concentrations were determined spectrophotometrically as described [34]. All proteins were used within 2 weeks after their production. The different mutants were produced by site-directed mutagenesis using QuickChange

protocols with the following primers (only the forward primers are given): M134S: 5′-CTGGGGAGTGCCTC CTCTAGACCCATG-3′; M154S: 5′-CTACCGTGAAAA CTCCAATCATACCC-3′; M206S: 5′-GACATCAAGA TATCCGAGCGCGTGG-3′; M213S: 5′-GTGGTGGAGC AGTCCTGTACCACCCAG-3′; M213L: 5′-GTGGTGAG CAGCTCTGTACCACCCAG-3′. The chain integrity of the different proteins was assessed during the experiments by SDS-PAGE using 15% acrylamide gels and Coomassie Blue staining procedures.

### Dynamic light scattering

Dynamic light scattering (DLS) measurements were carried out using the DynaPro Titan spectroscatter (Wyatt Technology) with controlled temperature and Dynamics software was used for data acquisition and analysis. All solutions (protein and buffers) were filtered through 0.22-μm Millex-GV filters. The samples (20 μl) were placed in a quartz cuvette and measured at a constant temperature of 15 or 25 °C, accumulating 20 measurements per sample. Values for the species hydrodynamic radius ($R_h$) and proportion (%) were derived from the autocorrelation data assuming a model of n-monodisperse globular proteins and using the software provided by the manufacturer. The data were compared by one-way ANOVA with Bonferroni′s post-test analysis using GraphPad Prism v 4.0.

### Circular dichroism

CD spectra were recorded using a Jasco-810 spectropolarimeter operating at 15°C and with 0.1 (far-UV, 250–200 nm) and 1 (near-UV, 320–250 nm) cm pathlength cuvettes. Approximately 13 μM (far-UV) and 30 μM (near-UV) protein concentration solutions were used. For each measurement, we averaged six scans. The data were corrected for the buffer components and then transformed into $\Theta_{mrw}$ using 110 as the mean residue molecular weight. Thermal denaturation experiments were performed by following the changes in the ellipticity ($\Theta$) at 222 nm as the samples were heated from 15 to 90°C at the rate of 1°/min. The reversibility of the secondary structure changes was assessed by comparing the spectra to those recorded after cooling to 15°C from 90°C. The changes in $\Theta^{222}$ with temperatures were normalized to the fraction of unfolded protein ($f_U$) using:

$$f_U = \left(\Theta^{222} - \Theta_N^{222}\right)/\left(\Theta_U^{222} - \Theta_N^{222}\right) \quad (1)$$

Here N and U refer to the native and unfolded states, respectively. The value of $f_U$ was plotted as a function of temperature for the calculation of Tm and ΔHm [35]. The experimental Tm values were converted into the apparent relative changes in free energy with respect to the wt protein ($\Delta\Delta G°_{MS/wt}$) using the equation:

$$\Delta\Delta G_{MS/wt} = \Delta Hm_{wt} \times [1 - Tm_{wt}/Tm_{MS}] \quad (2)$$

$Tm_{wt}$ and $Tm_{MS}$ are the Tm values for the wt and mutant protein, respectively, and $\Delta Hm_{wt}$ is the denaturation enthalpy of the wt protein [36, 37].

### Bis-ANS binding

Fluorescence emission spectra of bis-ANS (30 μM) were recorded in the presence and absence of 10–13 μM HaPrP(23–231) wt and its mutants using an SLM 8100 spectrofluorimeter equipped with a thermostated cell-holder. Spectra were recorded using 0.5-cm square cuvettes and an excitation wavelength of 380 nm. After correction for the buffer contribution and instrumental factors, we plotted the intensity at 470 nm as a function of temperature.

### Protein aggregation analysis

Protein solutions at various concentrations were prepared in 20 mM MES pH 6.5, 50 mM NaCl, 0.1 mM citrate and 0.03% $NaN_3$. After increasing the salt concentration to 0.35 M NaCl on ice, the solutions were incubated at 37°C under continuous orbital agitation at 100 rpm (unless stated otherwise). The samples were then analyzed for turbidity and protein solubility at different times. The turbidity was determined from absorbance readings at 450 nm using 0.5-cm quartz cuvettes in an Ultrospec 3000Pro equipped with a thermostated cell holder [34]. Protein solubility was determined from the partition of the protein between the supernatant and the soluble phase during centrifugation at 13,000 × *g* for 10 min at 4°C [38].

### Thioflavin T binding

The kinetics of thioflavin T (ThT) binding were monitored by bottom reading of fluorescence intensity in a POLARstar microplate reader (BMG Labtech) using 450-nm excitation and 480-nm emission filters, 0.20-ml samples and 15 μM ThT concentration. For best reproducibility, the reaction mixtures were prepared at 4°C into wells of black 96-well plates (Corning), sealed with foiled film and placed into the reader at 37°C to start the measurement. The measurement program consisted of ten flashes reading every 10 min with 1-min of orbital 1-mm diameter shaking at 100 rpm. The dead time between the preparation of the protein and the start of the measurement was usually 10 min. All measurements were done in triplicate and the experiments were repeated at least twice using two different protein batches. When required, the lag-phase was determined as described [39].

Atomic force microscopy

Typically, 2 µl of the protein solutions was diluted 1:50 with $H_2O$ after 24 h of polymerization reaction and deposited onto freshly cleaved mica surfaces. The samples were allowed to adsorb for 15 min and then were washed extensively with $H_2O$ and dried with a gentle stream of $N_2$. Atomic force microscopy (AFM) studies were performed using a PicoSPM LE AFM scanner (Molecular Imaging, Phoenix, AZ, USA) in acoustic alternating current mode with Si,N-ACT type cantilevers (ScienTec) that had a tip radius <10 nm and a spring constant of 25–75 N/m. The images (1 × 1 µm scans) were collected at a scan rate of 0.7–1 lines/s and analyzed using WSxM 5.0 Nanotec software.

## Results

MD simulations reveal that the M-to-S replacements perturb the PrP native state

Despite the chemical differences of the side-chain functional groups, M-to-S mutations provide the polar change of the sulfoxidation of methionine side chains while retaining the secondary structure propensities [27, 28]. To determine whether this polar substitution also behaves as a structural destabilizer, we first analyzed the impact of the mutations on the dynamic evolution of the C-terminal domain α-fold via MD simulations (Fig. 1). To compare the results with those previously obtained for the sulfoxide-variants, we performed this analysis using the 3D structure of HuPrP(125–229) and with its M206S, M213S, and M206S-M213S mutants [14].

First, we investigated the effect on the global dynamic properties. To this end we used essential dynamics (ED) analysis to identify concerted, non-random structural fluctuations in the proteins [40]. The analysis is based on the covariance-matrix of the positions of pairs of residues that can be extracted from each simulation. By focusing on the subset of the principal eigenvalues and eigenvectors of the covariance matrix, it is possible to define the "essential subspace" of the protein (generally correlated with the functional aspects of the conformational dynamics) and use the RWSIP (root weighted square inner product) parameter to calculate variations ([41], Table 1). A RWSIP value of 1 between two simulations would indicate that they are spanning identical conformational spaces, whereas a value

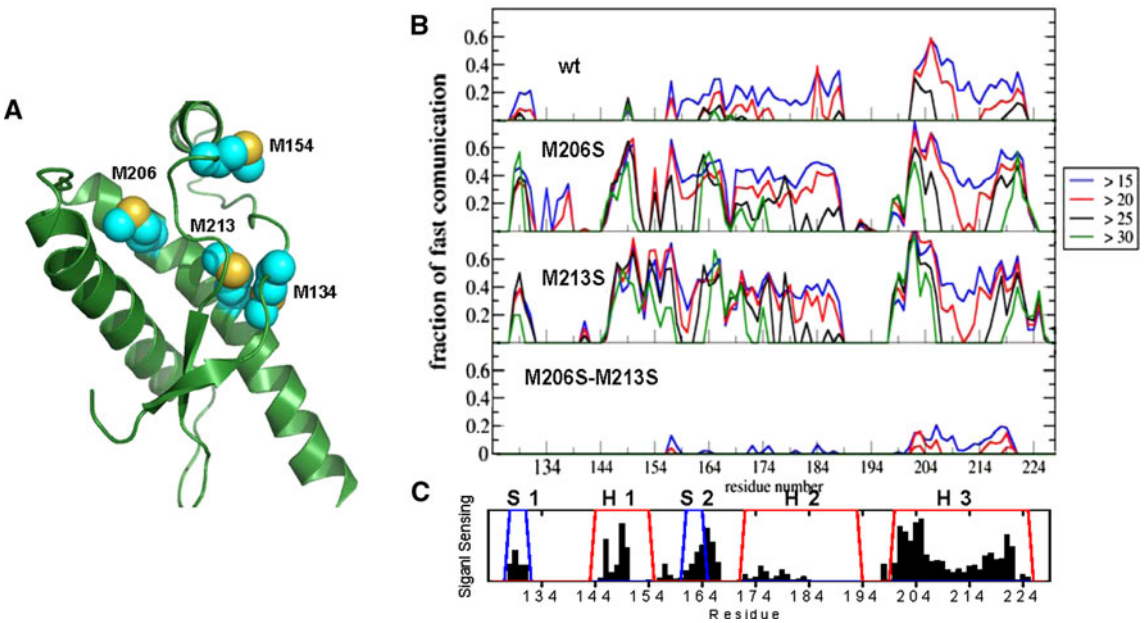


**Fig. 1** The relative dynamic effects of the substitution of the conserved Helix-3 Met by Ser in the HuPrP(125–229) α-fold, as analyzed by using MD. **a** The location of M134, M154, M206, and M213, the conserved methionines within all mammalian species studied, in the 3D structure of the HuPrP(125–229) α-fold. **b** The effects of the M-to-S mutations on the internal dynamic of the protein followed by the communication efficiency of all residues at increasing distances. Each bin refers to a residue and shows the fraction of residues of the whole protein that are highly prone to communicate with it (CP < 0.025). In each histogram, only communications at distances greater than a given threshold (>15, >20, >25, and >30 Å) are considered. **c** The signal sensing of the Helix-3 on M206 and M213 sulfoxidation. The variation of the fraction of residues with high CP in the M206 and M213 sulfoxidated chain with the residue number was taken from [14] and averaged for the distances. The regions corresponding to native strands (*blue*, S1,S2) and helices (*red*, H1,H2,H3) are highlighted. The unmodified protein is indicated as wt, whereas the mutated and oxidized forms are indicated as M-to-S or MO, respectively, together with the location (position 206, 213, or both)

**Table 1** Similarities and differences between the essential subspaces spanned by sulfoxidized (MO) and M-to-S mutant HuPrP (125–229) chains analyzed with the RWSIP values

| | wt | MO206 | MO213 | MO206, MO213 | M206S | M213S | M206S, M213S |
|---|---|---|---|---|---|---|---|
| wt | 1 | 0.65 | 0.63 | 0.51 | 0.65 | 0.70 | 0.51 |
| MO206 | | 1 | 0.42 | 0.54 | 0.68 | 0.61 | 0.50 |
| MO213 | | | 1 | 0.25 | 0.63 | 0.75 | 0.70 |
| MO206, MO213 | | | | 1 | 0.51 | 0.65 | 0.45 |
| M206S | | | | | 1 | 0.77 | 0.65 |
| M213S | | | | | | 1 | 0.63 |
| M206S, M213S | | | | | | | 1 |

Values refer to the RWSIP parameter calculated as described [41]. A value equal to 1 indicates that the two dynamic subspaces are identical, while a parameter value equal to 0 indicates absence of any superposition. The calculations were carried out on the combined trajectories for each of the mutants. Site of modification or mutation is indicated with the residue number

of 0 indicates the absence of superposition in the dynamic evolution of the systems. According to these metrics, the introduction of a single M-to-S mutation at positions 206 or 213 or a single sulfoxidation occurs with a comparable reduction in the similarity of the dynamic subspaces with the wt protein, with RWSIP values around 0.65 (Table 1). Interestingly, very similar low RWSIP values are observed for the double M-to-S mutation and for the double sulfoxidation variants. These results support that single and double M-to-S mutations perturb the conformational dynamic evolution of the native fold, a property previously found for the sulfoxidated forms [14].

To further determine whether the mutation can actually mimic the global dynamic effects of the oxidation, we calculated the RWSIP-based similarities of the essential subspaces spanned by the mutants and the sulfoxidized variants on the combined trajectories. Indeed, the RWSIP between the dynamics of the single variants at position 206 (M206S and M206MO) yielded a value of 0.68, and the RWSIP value calculated between the dynamics of the single variants at position 213 (M213S and M213MO) yielded a value of 0.75. The superposition of the essential subspaces of the double mutants is lower than for the previous cases, with an RWSIP value of 0.45. These latter results indicate that the perturbation introduced by double mutations forces the protein to sample different regions of the conformational space. In either case, M-to-MO or M-to-S substitutions, the double substitution variants span essential dynamic spaces that diverge from the native one. As a caveat, it should be considered that the simulation length, while being long compared to those currently run, may not be fully converged or may not have fully sampled all the relevant regions of the phase space. Taken together, these results show that M-to-S replacement, as M-to-MO, reduce the similarity of the dynamic subspaces to those of the wt protein, and that, for changes at the same positions, the similarity between the mutation and the oxidation decreases in the order from 213 > 206 > 206–213.

We next analyzed the differential effects on the internal dynamics of the protein (Fig. 1b). For this purpose, we calculated the communication propensity (CP) histograms of the different mutants of the protein according to the method described [14]. Each bin in the histogram represents the fraction of residues that have high communication efficiency with a given residue (CP < 0.025) among those with a distance higher than a certain threshold (i.e., 15, 20, 25 or 30 Å) from that residue. The value associated with each bin indicates the degree of coordination of that specific residue with the rest of the protein. It must be noted that the number of residues that communicate efficiently (y-axis) with a certain target residue (x-axis) represents a reverberation of the degree of internal coordination of the residue–residue pairs in a protein structure and it reports on the possible diffusion of dynamic effects due to specific perturbations. In this context, these calculations provide a qualitative view of the role of a region as a signal sensor, the signal being in this case a change in the chemical group. Interestingly, single M-to-S mutations at positions 206 and 213 increase the communication propensity mainly at longer distances of residues located at the N-terminal flank of the Helix-3, at the residues connecting the Strand-2 with Helix-2, and at the residues forming Helix-1. Strikingly, the double mutation to S in the M206S-M213S variant results in an almost complete abrogation of the native communication propensities among pairs of residues. Even at short threshold distances, communication is lost and no residue pairs are found to communicate efficiently. These results indicate that the double mutation severely perturbs the coordinated dynamics of the native fold, compared to the wt case, allowing the protein to visit alternative dynamic states, characterized by the lack of long-range communications between residue pairs. The latter data should, however, not be considered as a reverberation of the additive effect of the double M-to-S mutations: the perturbation introduced by the double mutation has an effect that is not limited to a "linear

combination" of the effects of the single mutations. As shown in the case of the RWSIP calculations, the double mutation determines a complex modulation of the dynamics that can be (partially) captured by investigating the degree of correlated and coordinated motions that characterize the mutated proteins. Summarizing, these data show that the M-to-S substitutions indeed trigger transmissible structural signals as found for the oxidative modifications [14].

Then, the emerging picture is that the polarity increase in the side chain provided by the M-to-S replacement perturbs the global coordination and essential dynamics of the α-fold native state. However, its destabilizing potency differs from that observed for the sulfoxidation of equivalent methionines.

## M-to-S mutations in Helix-3 distort the HaPrP(23–231) α-fold

The 3D structures of the globular domain of both HuPrP and HaPrP, and in particular the environments of M206 and M213, are highly conserved (Fig. 2a). The root mean squared deviation (RMSD) between the two 3D structures is 1.5 Å. The residues in Van der Waals contact with M213 [208-VVEQ-CITQ-217; 158-PNQV-161; 134-MSRP-136 in HuPrP(125–229)] are identical in both protein structures. The residues in contact with M206 [202-DVKM-ERVVE-211; F198; H187; I184 and 157-YP-158 in HuPrP(125–229)] differ only in respect to residues 203 (V/I Hu/Ha) and 205 (M/I Hu/Ha). It can therefore be assumed that the general trend of the structural perturbations induced by the polarity increase in the Helix-3-conserved Met residues should be species-independent.

Based on the previous considerations, we generated the full-length M206S, M213S, and M206S-M213S mutants using the HaPrP(23–231) wt chain as a template (Fig. 2a). We included the M134S and M154S mutations, as these residues are also conserved and flank secondary structure elements (Strand-1 and Helix-1, respectively). In addition, we prepared the mutant M213L as a control for site substitution (Figs. 1a, 2c). All these chains were produced in *E. coli* inclusion bodies, isolated under denaturing conditions and folded to the α-form [29, 34]. The chain integrity was assessed during experiments by SDS-PAGE (Fig. 2d).

We began the study of the effect of the M-to-S mutations on the conformation and stability of the HaPrP(23–231) α-fold using dynamic light scattering (DLS). In general, DLS provides information on the homogeneity and particle size of the protein solutions that can be transformed into molecular-sized species provided that hydrodynamic models are available. Despite the structural divergence of α-HaPrP(23–231) wt from classical globular

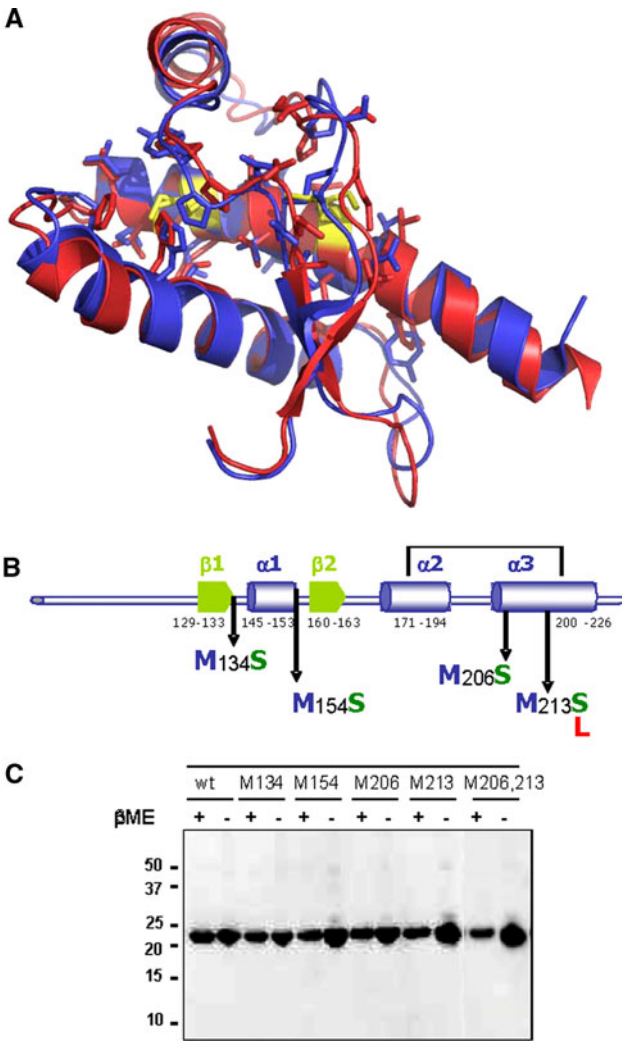


**Fig. 2** Pseudosulfoxidation mutants of HaPrP(23–231). **a** Overlapped 3D structures of the HuPrP (*red*) and HaPrP (*blue*) globular domains. Residues in Van der Waals contact with M206 and M213 are highlighted. **b** The HaPrP(23–231) mutant design. **c** PAGE-SDS analysis of HaPrP(23–231) wt and its M134S, M154S, M206S, M213S, and M206S-M213S used in the study, both in the absence and presence of *β*-mercaptoethanol. The M213L mutant yielded identical results

proteins and flexible polymers (the N-terminal domain is flexible and the C-terminal domain is globular), its monomeric behavior at pH 4.5 at protein concentrations up to 0.8 mM allows the determination of the $R_h$ for the monomer. This can be used as an internal control for variations ([42] and references therein). As depicted in Table 2, and at pH 4.5 and at 15°C, all proteins being studied yield an $R_h$ of about 3.7 ± 0.5 nm. Therefore, they can be described essentially as monomers. However, only the M206S, M213S, and M206S-M213S mutants permit the detection of an additional minor species (amounting to about 15% of the total) featured by a higher $R_h$ (9.2 ± 0.4 nm), suggesting the presence of soluble

**Table 2** Particle sizing of α-HaPrP(23–231) wt and of its mutants by dynamic light scattering

| Temperature | 15 (°C) | | | | 25 (°C) | | | |
|---|---|---|---|---|---|---|---|---|
| HaPrP(23–231) | $R_{h1}^{a,c}$ (nm) | % | $R_{h2}^{b,c}$ (nm) | % | $R_{h1}^{a,c}$ (nm) | % | $R_{h2}^{b,c}$ (nm) | % |
| wt | 3.2 ± 0.2 | 95 ± 5 | | | 3.9 ± 0.5 | 95 ± 4 | | |
| M134S | 4.0 ± 0.6 | 94 ± 5 | | | 4.4 ± 0.2 | 89 ± 2 | 9.6 ± 0.6 | 11 ± 4 |
| M154S | 3.3 ± 0.5 | 95 ± 5 | | | 3.3 ± 0.2 | 80 ± 5 | 9.5 ± 0.4 | 20 ± 7 |
| M206S | 4.5 ± 0.5 | 91 ± 6 | 9.0 ± 0.6 | 9 ± 6 | 4.5 ± 0.2 | 24 ± 10 | 9.5 ± 0.3 | 76 ± 8 |
| M213S | 3.3 ± 0.2 | 85 ± 6 | 9.0 ± 0.2 | 15 ± 7 | | | 8.8 ± 0.2 | 98 ± 4 |
| M206S, M213S | 3.6 ± 0.3 | 87 ± 7 | 9.1 ± 0.2 | 13 ± 6 | | | 9.0 ± 0.1 | 97 ± 4 |
| M213L | 3.3 ± 0.3 | 96 ± 5 | | | 3.6 ± 0.4 | 96 ± 4 | | |

Displayed data correspond to measurements performed at pH 4.5. The values of the hydrodynamic radius ($R_h$) and the related proportion (%) were derived from the scattered function using the model of n-globular monodisperse particles provided by the manufacturer's software. Data collected at pH 6.5 were essentially similar to that at pH 4.5. Data were compared by one-way ANOVA with Bonferroni's post-test analysis

[a] Differences in the values of $R_{h1}$ were not statistically significant

[b] Differences in the values of $R_{h2}$ were not statistically significant

[c] Differences between $R_{h1}$ and $R_{h2}$ are statistically significant ($p < 0.01$)

oligomers (see below). Experiments performed at pH 6.5 yielded essentially similar results (data not shown).

The conformational features of HaPrP(23–231) wt and its M-to-S mutants were then studied by far- and near-UV CD to probe the secondary and tertiary structures, respectively (Fig. 3). At pH 4.5 and pH 6.5, a comparison of the far-UV CD spectra shows that only M206S and M213S mutations, singly or in combination, cause a drastic change (Fig. 3a, b). This change is characterized by an increase in the $\Theta^{205}/\Theta^{220}$ ratio (from 1.07 up to 2.0) and indicates the presence of non-native secondary structures. As in the previous spectral region, the M206S and M213S mutations, both singly or combined, also altered the near-UV spectrum. This is not true for the M134S and M154S mutations. Here the observed spectral changes, in which the aromatic bands but not the disulfide bond region (around 260 nm) are affected, show the disruption of the native tertiary structure (Fig. 3c). The CD studies taken together indicate that the replacement of M by S at positions 206, 213, and both, but not at positions M134 or M154, preclude the adoption of the conventional α-fold and induce partially unstructured states. Interestingly, replacing M213 by L rather than S retains the conformational features of the wt supporting the importance of the polarity of the side chain for the observed perturbations (Fig. 3a, b, and c).

To gain insight into the partially unfolded state induced upon mutation of the M-to-S in Helix-3, we characterized the bis-ANS binding properties, a probe that is used to titrate surface hydrophobicity [43]. Figure 3d shows that as opposed to HaPrP(23–231) wt, M134S, M154S, and M213L, the Helix-3 M-to-S mutants displayed an enhanced binding of bis-ANS, indicating an increase in their solvent-exposed hydrophobic surfaces and again their partially structured state.

### Thermal unfolding reveals the M-to-S replacements in Helix-3 cause a drastic reduction in thermal stability

Given that structural changes have large impacts on stability, we further probed the effect of the M-to-S substitutions using thermal denaturation experiments. Under the conditions used, the thermal unfolding of the wt, M134S, M154S, and M213L proteins, as followed by the variation of $\Theta^{222}$ as a function of temperature, was essentially reversible as judged from the recovering of approximately 95% of the initial signal on cooling from the highest temperature. The thermal unfolding curves for these proteins denote identical two-state processes with Tm′s of about 57 ± 1 at pH 6.5, whereas at pH 4.5 the M134S and M154S mutants unfold at a lower Tm than the wt (56 ± 0.5 and 61 ± 0.5°C, respectively) (Fig. 4; Table 3). Conversely, the thermal denaturation of M206S, M213S, and the M206S-M213S HaPrP(23–232) was only partially reversible (75% of the signal was recovered after cooling from the highest temperature), involved a lower $\Delta\Theta^{222}$, was less cooperative and occurred at significantly lower temperatures (38 and 40°C at both pH 6.5 and 4.5, respectively) (Fig. 4; Table 3).

All the features found for the Helix-3 M-to-S mutants follow the pattern for the thermal unfolding of partially unstructured states involving pro-aggregating species [44]. To assess this process, we studied the temperature dependence of bis-ANS binding and of the hydrodynamic radius (Figs. 2, 4c). In addition to the previously described differences in the temperature dependence of $\Theta^{222}$, the chains bearing M-to-S mutations at the Helix-3 methionines also displayed a temperature-dependent ANS binding and $R_h$ changes at low temperatures. These are not observed in HaPrP(23–231) wt, M134S, M154S, and M213L. In this

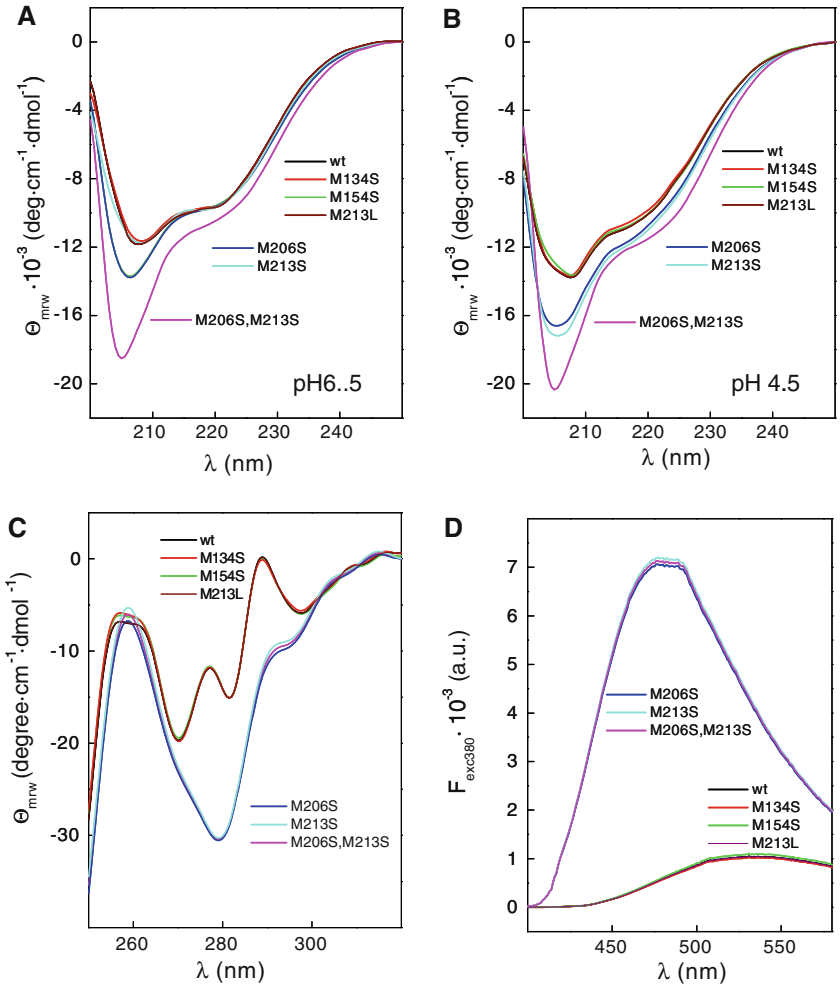


**Fig. 3** Conformational features of HaPrP(23–231) wt and of its mutants as probed by circular dichroism in the far-UV region (**a**, **b**) and near-UV region (**c**) and by their bis-ANS binding properties (**d**). Far-UV CD spectra of HaPrP(23–231) wt and of its mutants **a** in 20 mM MES pH 6.5 containing 50 mM NaCl and 0.1 mM citrate, and **b** 20 mM NaAc pH 4.5 containing 50 mM NaCl and 0.1 mM citrate. Spectra were recorded at 15°C using protein at 11 μM. **c** Near-UV CD spectra of the different HaPrP(23–231) chains. The spectra were recorded at 15°C using protein solutions at 22 μM. **d** The effect of HaPrP(23–231) wt and its mutants on the bis-ANS fluorescence emission spectrum at 15°C. The displayed data are the averaged of three independent measurements using at least two different protein batches The trace color or symbol codes are indicated in each of the panels

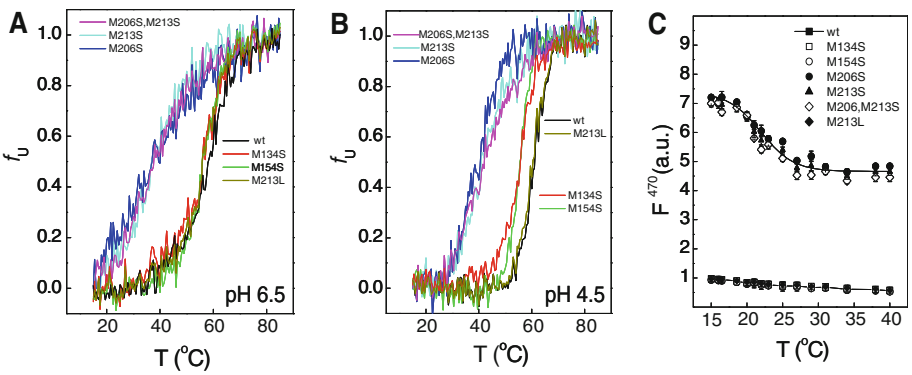


**Fig. 4** The thermal unfolding profiles of HaPrP(23–231) wt and of its mutants as monitored by circular dichroism and ANS-binding. The temperature dependence of the $\Theta_{222}$ for HaPrP(23–231) wt and of its mutants, at pHs: **a** 6.5 and **b** 4.5. The trace color code is indicated in each of the panels. **c** The temperature dependence of the ANS emission intensity in the presence of HaPrP(23–231) wt and its mutants

sense, the bis-ANS-binding profiles show sigmoidal decays with inflection points at approximately 21 ± 1.5°C, indicating that the Helix-3 methionine mutants undergo a transition involving the reduction in the hydrophobic surface. This transition is accompanied by a threefold increase in the $R_h$ value and precedes the temperature-dependent changes in the secondary structure (Table 2; Fig. 4). These data suggest the presence of pro-aggregating folding intermediates.

The differences in the reversibility of the thermal unfolding processes preclude any formal equilibrium thermodynamic analysis. However, given the reversibility of the HaPrP(23–231) wt thermal denaturation at both pHs allows the calculation of the thermodynamic parameters at equilibrium (ΔHm). Given this fact, the experimental Tm values for the denaturation of the different mutants can be converted into the apparent relative changes in the free energy with respect to the wt protein [36, 37]. Table 3

**Table 3** Parameters of the thermal unfolding of HaPrP(23–231) wt and of its mutants followed by the variation of $\Theta^{222}$ with temperature

| | pH | Tm (°C) | $\Theta_{15}^{222}$ (deg cm$^{-1}$ dmol$^{-1}$) | $\Theta_{90}^{222}$ (deg cm$^{-1}$ dmol$^{-1}$) | ΔT (°C) | $\Delta G^*_{MS/wt}$ (kcal mol$^{-1}$) |
|---|---|---|---|---|---|---|
| wt | 6.5 | 57.8 ± 0.5 | −9.3 ± 0.2 | −5.7 ± 0.1 | 5 ± 1 | |
| | 4.5 | 60.9 ± 0.4 | −9.4 ± 0.3 | −7.3 ± 0.1 | 3 ± 0.5 | |
| M134S | 6.5 | 57.0 ± 0.5 | −9.2 ± 0.5 | −5.5 ± 0.2 | 5 ± 1 | −0.10 ± 0.09 |
| | 4.5 | 55.4 ± 0.5 | −9.1 ± 0.5 | −6.7 ± 0.2 | 3 ± 0.5 | −1.11 ± 0.06 |
| M154S | 6.5 | 56.3 ± 0.4 | −9.2 ± 0.3 | −5.5 ± 0.2 | 4 ± 1 | −0.20 ± 0.10 |
| | 4.5 | 55.5 ± 0.6 | −9.3 ± 0.3 | −6.7 ± 0.3 | 2 ± 0.6 | −1.05 ± 0.06 |
| M206S | 6.5 | 37.9 ± 0.2 | −9.5 ± 0.4 | −7.4 ± 0.5 | 10 ± 0.5 | −3.30 ± 0.12 |
| | 4.5 | 39.5 ± 0.3 | −10 ± 0.2 | −7.9 ± 0.5 | 5 ± 0.4 | −4.45 ± 0.09 |
| M213S | 6.5 | 38.1 ± 0.9 | −9.4 ± 0.4 | −7.2 ± 0.4 | 7 ± 0.6 | −3.20 ± 0.11 |
| | 4.5 | 41.0 ± 1.0 | −10.2 ± 0.2 | −8.7 ± 0.4 | 5 ± 0.4 | −4.13 ± 0.09 |
| M206S,M213S | 6.5 | 36.7 ± 0.9 | −10.0 ± 0.2 | −7.4 ± 0.4 | 10 ± 0.5 | −3.50 ± 0.10 |
| | 4.5 | 42.0 ± 1.0 | −11.0 ± 0.2 | −9.4 ± 0.4 | 10 ± 0.5 | −3.93 ± 0.04 |
| M213L | 6.5 | 58.8 ± 1.0 | −9.4 ± 0.3 | −5.6 ± 0.2 | 3 ± 0.5 | 0.15 ± 0.09 |
| | 4.5 | 60.5 ± 0.4 | −9.2 ± 0.3 | −7.3 ± 0.1 | 3 ± 0.5 | −0.08 ± 0.07 |

Thermal unfolding curves were analyzed as described in the experimental section. $\Delta G^*_{MS/wt}$ were calculated using the $\Delta H_{vH}$ (50.8 kcal/mol and 65.5 kcal/mol for pH 6.5 and 4.5, respectively) calculated from the thermal denaturation curves of HaPrP(23–231) wt analyzed according to a two-state transition. $\Theta_{15}^{222}$ and $\Theta_{90}^{222}$ represent the values of ellipticity at 15 and 90°C, respectively. ΔT was derived from the fit to sigmoidal curves to estimate changes in the cooperativity of the transitions

shows that all the M-to-S replacements cause changes in stability, ranging from −0.20 ± 0.10 to −4.45 ± 0.09 kcal mol$^{-1}$. For the M134S and M154S mutants, the destabilization of the secondary structure is only significant at pH 4.5. For the Helix-3 methionine mutants, the destabilization is larger and involves relative changes in the apparent free energy of −3.20 and −4.5 kcal mol$^{-1}$, respectively. Contrarily, the M213L mutation causes negligible effects. Taken together, these results indicate that the M-to-S substitutions in Helix-3 do indeed prevent the adoption of the conventional α-fold and induce a partially structured state.

## Helix-3 M-to-S mutants of HaPrP(23–231) undergo facilitated aggregation and fibrillation

Bearing in mind that partially structured states are key precursors for the formation of amyloid fibrils through their allowance for rearrangement of "amyloid-prone sequence regions" [9, 11, 16, 18, 45], we then asked whether the structural states formed by M-to-S replacement in Helix 3 could permit or facilitate oligomerization pathways that are impeded to the native fold. For this purpose, we incubated HaPrP(23–231) wt and its mutants in 20 mM MES pH 6.5, 0.1 mM citrate and 0.01% $NaN_3$ in the absence and presence of 0.35 M NaCl at 37°C with orbital agitation. The samples were analyzed for the occurrence of polymerization processes (Fig. 5).

The aggregation kinetics, followed by turbidity measurements, show that all proteins at concentrations above 13 μM undergo a time-dependent aggregation upon increasing the ionic strength to 0.35 M NaCl (Fig. 5a). However, the turbidity increase was significantly larger for the Helix-3 methionine mutants than for the wt, M134S, M154S, and M213L mutants. The turbidity changes paralleled the formation of insoluble aggregates. The solubility, measured after 24 h of incubation, shows that aggregation was significantly larger for the Helix-3 methionine mutants than for the wt, M134S, and M154S HaPrP(23–231) proteins (Fig. 5c). Under similar conditions, the kinetics of ThT binding reveal the occurrence of a significant fibrillation process in the M206S, M213S, and M206S-M213S mutants. This process was negligible in the wt, M134S, M154S, and M213L HaPrP(23–231) forms (Fig. 5b). The degree of probe binding in the isolated insoluble polymers was essentially similar to the three different M-to-S Helix-3 mutants (Fig. 5d). Similarly, the lag-phase for this process, calculated using three independent experiments with protein concentrations of about 14 ± 1 μM, yielded values of 2.5 ± 0.5 h for the three different M-to-S Helix-3 mutants.

To assess the nature of the protein polymers formed after 24 h of incubation, we analyzed the morphology using AFM. Analyzing the topographical images of the Helix-3 methionine mutants revealed the presence of aggregates constituted by irregular rod-like structures with diameters of about 25–50 nm and typical lengths of a few hundreds of nanometers (Fig. 6). These formations appeared heterogeneous, and included single straight rods, laterally associated rods, doughnut, and hairpin-like shapes. This precluded the detection of clear-cut differences among the distinct Helix-3 methionine mutants and

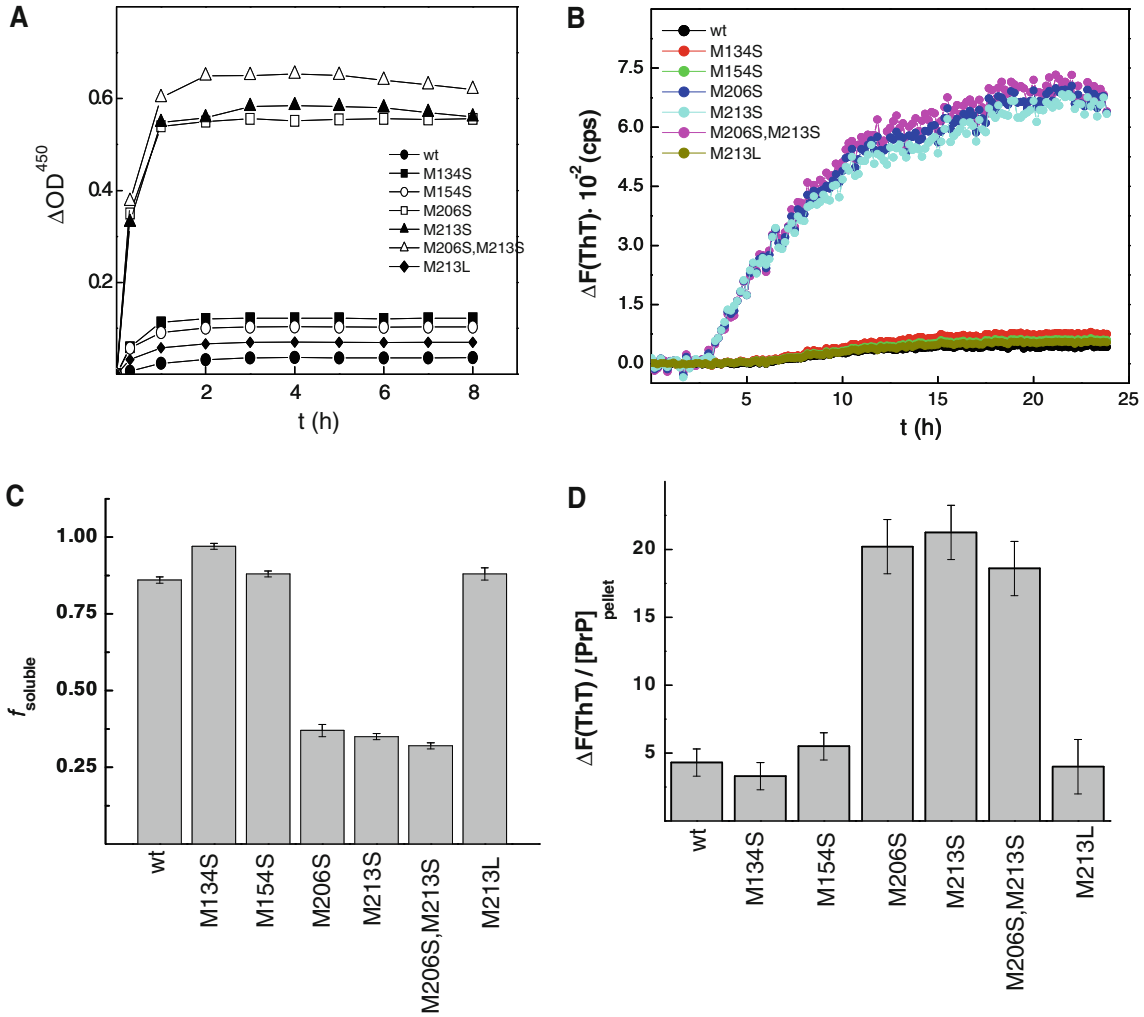


**Fig. 5** The aggregation properties of HaPrP(23–231) wt and its M-to-S mutants. **a** The time-dependence of the turbidity increase of the different protein solution solutions prepared in 20 mM MES, 0.35 M NaCl, 0.1 mM citrate, and 0.01% $NaN_3$ at pH 6.5, upon incubation at 37°C under agitation. **b** Typical kinetics of the ThT binding of HaPrP(23–231) wt and its mutants. The displayed traces are the averaged of three independent experiments performed in triplicate. **c** The partition of HaPrP(23–231) wt and its mutants into the soluble fraction during a 10,000 × g centrifugation for 20 min after a 24-h incubation under aggregating conditions (37°C, 0.35 M NaCl). Solubility is expressed as the molar fraction of the total protein concentration (approximately 13–14 μM) and represents the average of two independent determinations with different protein batches using duplicates. **d** The extent of ThT in isolated insoluble aggregates. The insoluble aggregates formed after 24-h incubation were isolated by centrifugation, resuspended in the same buffer, and the ThT fluorescence was referred to the protein concentration. The data are displayed as the average of three independent measurements performed in triplicate

suggested similarity with prefibrillar states [46, 47]. It must be stressed that despite the polymorphism of the assemblies formed by the M206S, M213S, and M206S-M213S mutants, their shapes were clearly different from the amorphous patches formed by HaPrP(23–231) wt, used as control for adherence. Measurements from cross sections of the isolated assemblies of the mutants yielded averaged values of 4.0 ± 0.4 nm for the height (Fig. 6). Correction of these values for the dehydration effect (multiplying by a factor of 1.4 [47]). the heights of the assemblies (5.6 nm) agree with the diameters of protofibrils, which are typically of 2–6 nm [46, 47].

In conclusion, these results indicate that under denaturant-free conditions, the partially structured state that is induced by the M-to-S substitution in Helix-3 undergoes a polymerization process leading to the formation of amyloid protofibrils.

## Discussion

The conversion of $PrP^C$ into its propagative $PrP^{Sc}$ form involves a drastic structural change that requires the remodeling of the noncovalent bonds of at least its

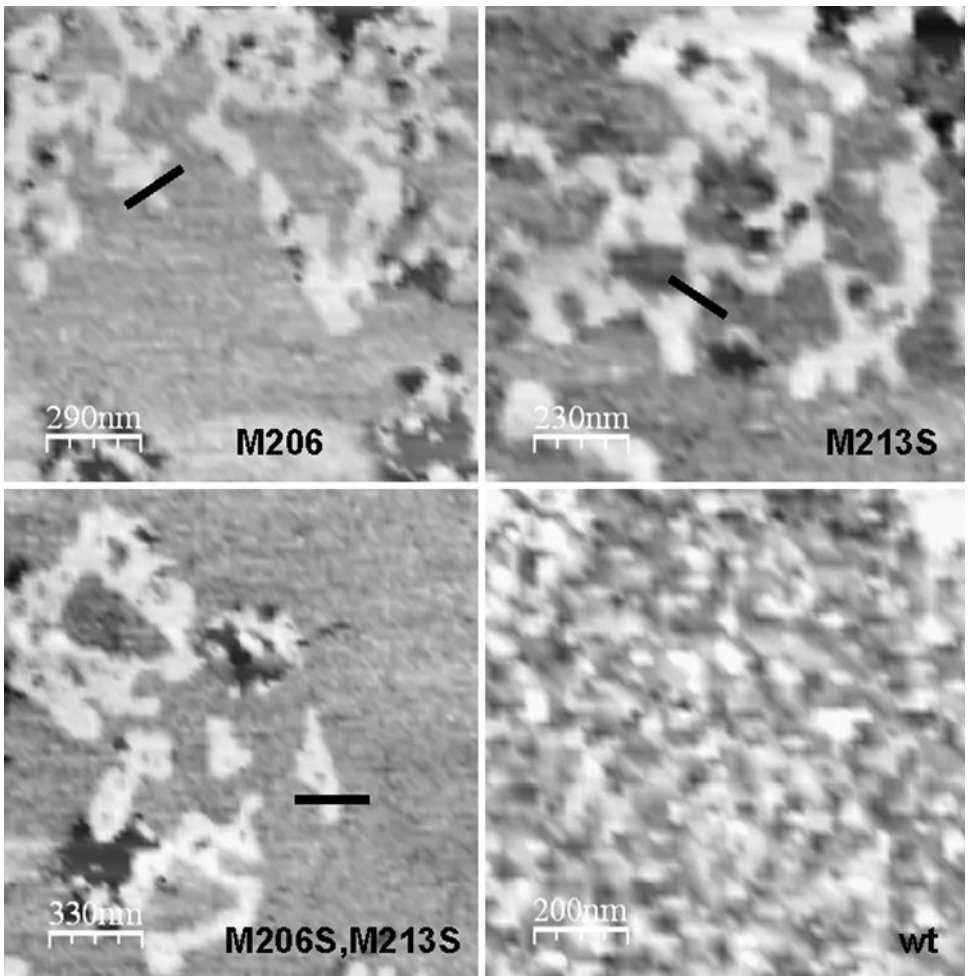


**Fig. 6** AFM topographical images of amyloid polymers adsorbed onto mica surfaces. The AC-AFM topographic image of aggregates formed by **a** M206S, **b** M213S, **c** M206-M213S mutants and **d** wt chains of HaPrP(23–231) after 24-h incubation at 0.4 mg/ml at 37°C in 20 mM MES, 0.35 M NaCl, 0.1 mM citrate, and 0.01% $NaN_3$, at pH 6.5, under agitation at 100 rpm. Scans were registered at 1 × 1 μm. Z range (black to white) is 10 nm on average. *Black bars* indicate example of regions selected as cross sections for height determinations

C-terminal domain. To do so, the α-fold of PrP must undergo an obligatory destabilization (i.e., breakage of noncovalent bonds) and accommodate into an aggregation-prone state (or ensemble of states) that may allow the efficient formation of new noncovalent bonds [9, 18]. Within this picture, the finding of sulfoxides at the Helix-3 methionines in $PrP^{Sc}$, which provide an increase in local polarity with transmissible structural effects, offered an adequate covalent feature for switching on either the formation or stabilization of the obligatory folding intermediate [12–14]. If transient, this intermediate can be a physiological form of $PrP^{C}$ (for example, as a species on the pathway to degradation). However, if accumulated, the intermediate could evolve to $PrP^{Sc}$. Using mutagenesis to provide a side-chain polarity increase with site specificity, our work shows that M-to-S replacements at Helix-3 disrupt the native protein fold. This forces the full-length chain to adopt a partially structured fold that forms amyloid protofibrils through its pro-aggregation properties. Interestingly, such structural effects are not observed when the replacement is performed at the conserved M134 and M154 residues or when M213 is replaced by L rather than S. This supports the specificity of the target sites and of the polarity change.

The analysis by MD simulations shows that the M-to-S mutations perturb both the global and internal dynamics of the native state. Single M-to-S substitutions determine effects on the global dynamics and on the internal coordination of the α-fold that are similar to the effects observed for the sulfoxidation of the respective methionines. This qualitatively supports the possibility to mimic methionine sulfoxidation by serine substitution. The effect of the double M-to-S mutations is more complex and determines a perturbation of the native state dynamics that reverberates in a different sampling of essential spaces and in a complete abrogation of internal residue-pair coordination. These results should not be considered as fully quantitative, given the inherent limitations of the force-fields and of the sampling. However, they indicate that the insertion of an electronegative oxygen atom in an otherwise mainly hydrophobic environment may act as a possible switch for the control of the conformational stability of the protein. The differences in the outcomes of methionine sulfoxidation or M-to-S substitutions can be

explained in terms of the disparity in the chemical groups and of the trajectory length for each of the groups required to display the effect. However, the fact that the M-to-S substitution in Helix-3, which theoretically is less perturbing than sulfoxidation experimentally impairs the adoption of the native state in the full-length chain, also argues for alternative destabilizing sources eluded in the theoretical approach. This means that the effect of the substitutions on stability factors provided by other protein regions, by alternative dynamic states or by both, that are not computed, are indeed playing a critical role in the final outcome. In this sense, it must be noted that the unstructured N-terminal region plays an important role in the structure and stability of $PrP^C$ and of its conversion capacity and it is not included in the structure of the native state [27, 48]. It must also be considered that the effects of the substitutions could a priori differ in the effects on the native-state properties but could converge in stabilizing folding intermediates [49, 50].

Folding intermediates or partially structured species are usually very short-lived and less stable than the fully folded form, and so they are not significantly populated at equilibrium. Conversely, stable conformations of proteins that are not fully folded or unfolded can be found under several non-native conditions, for example at extreme pHs, mild denaturant concentrations, loss of cofactors, and upon engineering certain residues [22, 49, 50]. Most of these states retain considerable native-like secondary structure but have disrupted tertiary structure [47, 49]. In general, these partially structured states allow the expansion of the structural and functional repertoire through their increased flexibility. Loss of the cation cofactor and acid pHs permits α-lactalbumin to adopt a folding intermediate that yields the antitumoral form referred to as HAMLET upon oleic acid binding [51]. Similarly, mild denaturing conditions permit Rop-dimer interconversion between two opposed native structures [52]. From this work, it can be proposed that the pseudosulfoxidation mutations in Helix-3 act as trapdoors for the formation of partially structured states that can easily evolve to protofibrils. However, it could be possible that such intermediates could be either degraded or rescued by ligand binding and yield novel functions in the cellular milieu [23, 24, 53].

In general, the accumulation of covalent modifications appears to be both the cause and a consequence of ageing and a crucial factor contributing to neurodegenerative disease pathogenesis through either the impairment of their reversibility or their occurrence at alternative sites [21, 23, 25]. In the case of tau-related dementias, hyperphosphorylation impairs microtubule-binding function and causes the protein to accumulate as neurofibrillary tangles [20, 21]. Importantly, the changes in the properties of tau that occur on hyperphosphorylation can be reproduced or mimicked using S/T-to-E mutations [22]. For Aβ-peptides and ApoC-II, methionine sulfoxidation favors the formation of non-amyloid oligomeric states [30, 51, 52]. In the case of PrP, the use of site-specificity for the polarity replacement shows that only the oxidation of hidden methionines, M206 and M213, would have deleterious consequences for the α-fold. Assuming that these methionines can be transiently exposed through the perturbation of Helix-3 (as shown by high-pressure studies [54] or in states populated in pathways to degradation), the sulfoxide-stabilized state could be then considered as a physiological folding intermediate. Its accumulation would then favor the pathway of conversion through the impairments of its reversion and degradation [23, 24].

The work with synthetic peptides has shown that the redox cycle of methionine side chains involves an amphipathic code that can function as a structural switch regulating not only the secondary structure but also the shape of the peptide oligomers [27, 28, 55, 56]. Given the high content of methionine residues in the PrP chain and their differences in location and conservation degree, it may be possible that these residues participate in a general evolutionary mechanism involved in the regulation of the folding basin. In this sense, the site-specificity conferred by the mutational approach described here, which is in contrast to the lack of specificity of the chemical oxidation and the variability of its effect [57, 58], indicates that the polarity increase linked to the oxidation of M206 and M213, but not that of M134 and M154, is critical for the permissibility of the native α-fold. The polarity effect also plays a role in polymer sculpturing, as pseudosulfoxidation of the Helix-3 methionines stalls the polymerization process at the protofibril stage. In addition to M206 and M213, some species contain an extra Met residue in Helix-3 (M205, in human and mouse, among others) that is essential for proper folding and that when mutated switches on the aggregation propensity of the C-terminal domain, reinforcing the α-fold gatekeeper role of Helix-3 methionines [59]. On the other hand, M129 which is highly conserved, but polymorphic in human (M129V) and deer (M132L), was found as easily oxidized as M134 [57]. Preventing such oxidation sensitivity as in the polymorphic variant V129 does not cause major conformational effects or preclude succumbing to diseases but indeed modulates the risk and phenotype of prion disorders in humans in agreement with the previous hypothesis [59]. In cervid PrP the polymorphism M132L, which dictates the oxidation capacity of the position, determines the strain susceptibility [60].

Then, deciphering this as yet unresolved code may be of essential importance for understanding the regulation of the folding basin of proteins in relation to their misfolding in terms of both the permissibility of conformational transitions and the properties of their assemblies.

**Acknowledgments** This work was supported by grants SAF2006-00418 (MG) and BFU2009-07971 (MG) from the Ministerio de Ciencia e Innovación, FOOD-CT-2004-506579 (MG, RG) from the EC and PI101209 (MG) from the Fundación Cien. SL is supported by a FPI-PhD fellowship from the Ministerio de Ciencia e Innovación. We gratefully acknowledge the advice of Dr. Angel Cuesta in relation to the AFM experiments and the technical support of Lara Reviejo and Rosa Sánchez.

## References

1. Prusiner SB (2001) Shattuck lecture: neurodegenerative diseases and prions. N Engl J Med 344:1516–1526
2. Aguzzi A, Baumann F, Bremer J (2008) The prion's elusive reason for being. Annu Rev Neurosci 31:439–477
3. Oesch B, Westaway D, Wälchli M, McKinley MP, Kent SB, Aebersold R, Barry RA, Tempst P, Teplow DB, Hood LE, Prusiner SB, Weissmann C (1985) A cellular gene encodes scrapie PrP 27–30 protein. Cell 40:735–746
4. Meyer RK, McKinley MP, Bowman KA, Braunfeld MB, Barry RA, Prusiner SB (1986) Separation and properties of cellular and scrapie prion proteins. Proc Natl Acad Sci USA 83:2310–2314
5. Caughey BW, Dong A, Bhat KS, Ernst D, Hayes SF, Caughey WS (1991) Secondary structure analysis of the scrapie-associated protein PrP 27–30 in water by infrared spectroscopy. Biochemistry 30:7672–7680
6. McKinley MP, Meyer RK, Kenaga L, Rahbar F, Cotter R, Serban A, Prusiner SB (1991) Scrapie prion rod formation in vitro requires both detergent extraction and limited proteolysis. J Virol 65:1340–1351
7. Gasset M, Baldwin MA, Lloyd DH, Gabriel JM, Holtzman DM, Cohen F, Fletterick R, Prusiner SB (1992) Predicted alpha-helical regions of the prion protein when synthesized as peptides form amyloid. Proc Natl Acad Sci USA 189:10940–10944
8. Pan KM, Baldwin M, Nguyen J, Gasset M, Serban A, Groth D, Mehlhorn I, Huang Z, Fletterick R, Cohen F, Prusiner SB (1993) Conversion of alpha-helices into beta-sheets features in the formation of the scrapie prion proteins. Proc Natl Acad Sci USA 90:10962–10966
9. Baskakov IV, Breydo L (2007) Converting the prion protein: what makes the protein infectious. Biochim Biophys Acta 1772:692–703
10. Sigurdson CJ, Nilsson KP, Hornemann S, Heikenwalder M, Manco G, Schwarz P, Ott D, Rülicke T, Liberski PP, Julius C, Falsig J, Stitz L, Wüthrich K, Aguzzi A (2009) De novo generation of a transmissible spongiform encephalopathy by mouse transgenesis. Proc Natl Acad Sci USA 106:304–309
11. Colby DW, Giles K, Legname G, Wille H, Baskakov IV, Dearmond SJ, Prusiner SB (2009) Design and construction of diverse mammalian prion strains. Proc Natl Acad Sci USA 106:20417–20422
12. Stahl N, Baldwin MA, Teplow DB, Hood L, Gibson BW, Burlingame AL, Prusiner SB (1993) Structural studies of the scrapie prion protein using mass spectrometry and amino acid sequencing. Biochemistry 32:1991–2002
13. Canello T, Engelstein R, Moshel O, Xanthopoulos K, Juanes ME, Langeveld J, Sklaviadis T, Gasset M, Gabizon R (2008) Methionine sulfoxides on PrPSc: a prion-specific covalent signatura. Biochemistry 47:8866–8873
14. Colombo G, Meli M, Morra G, Gabizon R, Gasset M (2009) Methionine sulfoxides on prion protein Helix-3 switch on the alpha-fold destabilization required for conversion. PLoS One 4(1):e4296
15. Wolschner C, Giese A, Kretzschmar HA, Huber R, Moroder L, Budisa N (2009) Design of anti- and pro-aggregation variants to assess the effects of methionine oxidation in human prion protein. Proc Natl Acad Sci USA 106:7756–7761
16. Kelly JW (1998) The alternative conformations of amyloidogenic proteins and their multi-step assembly pathways. Curr Opin Struct Biol 8:101–106
17. Eisenberg D, Nelson R, Sawaya MR, Balbirnie M, Sambashivan S, Ivanova MI, Madsen AØ, Riekel C (2006) The structural biology of protein aggregation diseases: fundamental questions and some answers. Acc Chem Res 39:568–575
18. Nelson R, Eisenberg D (2006) Structural models of amyloid-like fibrils. Adv Protein Chem 73:235–282
19. Sawaya MR, Sambashivan S, Nelson R, Ivanova MI, Sievers SA, Apostol MI, Thompson MJ, Balbirnie M, Wiltzius JJ, McFarlane HT, Madsen AØ, Riekel C, Eisenberg D (2007) Atomic structures of amyloid cross-beta spines reveal varied steric zippers. Nature 447:453–457
20. Kopke E, Tung YC, Shaikh S, Alonso AC, Iqbal K, Grundke-Iqbal I (1993) Microtubule-associated protein tau: abnormal phosphorylation of a non-paired helical filament pool in Alzheimer disease. J Biol Chem 268:24374–24384
21. Iqbal K, Liu F, Gong CX, Alonso AC, Grundke-Iqbal I (2009) Mechanisms of tau-induced neurodegeneration. Acta Neuropathol 118:53–69
22. Sun Q, Gamblin TC (2009) Pseudohyperphosphorylation causing AD-like changes in tau has significant effects on its polymerization. Biochemistry 48:6002–6011
23. Stadtman ER (2006) Protein oxidation and aging. Free Radic Res 40:1250–1258
24. Oien DB, Moskovitz J (2008) Substrates of the methionine sulfoxide reductase system and their physiological relevance. Curr Top Dev Biol 80:93–133
25. Hernández F, Nido JD, Avila J, Villanueva N (2009) GSK3 inhibitors and disease. Mini Rev Med Chem 9:1024–1029
26. Virshup DM, Shenolikar S (2009) From promiscuity to precision: protein phosphatases get a makeover. Mol Cell 33:537–545
27. Ostapchenko VG, Makarava N, Savtchenko R, Baskakov IV (2008) The polybasic N-terminal region of the prion protein controls the physical properties of both the cellular and fibrillar forms of PrP. J Mol Biol 383:1210–1224
28. Dado GP, Gellman SH (1993) Redox control of secondary structure in a designed peptide. J Am Chem Soc 115:12609–12610
29. Schenck HL, Schenck HL, Dado GP, Gellman SH (1996) Redox-triggered secondary structure changes in the aggregated states of a designed methionine-rich peptide. J Am Chem Soc 118: 12487–12494
30. Binger KJ, Griffin MD, Howlett GJ (2008) Methionine oxidation inhibits assembly and promotes disassembly of apolipoprotein C-II amyloid fibrils. Biochemistry 47:10208–10217
31. Wiltzius JJ, Landau M, Nelson R, Sawaya MR, Apostol MI, Goldschmidt L, Soriaga AB, Cascio D, Rajashankar K, Eisenberg D (2009) Molecular mechanisms for protein-encoded inheritance. Nat Struct Mol Biol 16:973–978
32. Vriend G (1990) What if: a molecular modeling and drug design program. J Mol Graph 8:52–56
33. James TL, Liu H, Ulyanov NB, Farr-Jones S, Zhang H, Donne DG, Kaneko K, Groth D, Mehlhorn I, Prusiner SB, Cohen FE (1997) Solution structure of a 142-residue recombinant prion protein corresponding to the infectious fragment of the scrapie isoform. Proc Natl Acad Sci USA 94:10086–10091
34. González-Iglesias R, Pajares MA, Ocal C, Espinosa JC, Oesch B, Gasset M (2002) Prion protein interaction with glycosaminoglycan occurs with the formation of oligomeric complexes stabilized by Cu(II) bridges. J Mol Biol 319:527–540

35. Pace CN, Scholtz JM (1997) Measuring the conformational stability of a protein. In: Creighton (ed) Protein structure, a practical approach. IRL Press, Oxford, pp 299–321
36. Becktel WJ, Schellman JA (1987) Protein stability curves. Biopolymers 26:1859–1877
37. Tadeo X, López-Méndez B, Castaño D, Trigueros T, Millet O (2009) Protein stabilization and the Hofmeister effect: the role of hydrophobic solvation. Biophys J 97:2595–2603
38. González-Iglesias R, Elvira G, Rodríguez-Navarro JA, Vélez M, Calero M, Pajares MA, Gasset M (2004) $Cu^{2+}$ binding triggers alphaBoPrP assembly into insoluble laminar polymers. FEBS Lett 556:161–166
39. Bishop MF, Ferrone FA (1984) Kinetics of nucleation-controlled polymerization: a perturbation treatment for use with a secondary pathway. Biophys J 46:631–644
40. Amadei A, Linssen ABM, Berendsen HJC (1993) Essential dynamics of proteins. Proteins 17:412–425
41. Carnevale V, Pontiggia F, Micheletti C (2007) Structural and dynamical alignment of enzymes with partial structural similarity. J Phys Condens Matter 19. doi:10.1088/0953-8984/19/28/285206
42. Lysek DA, Schorn C, Nivon LG, Esteve-Moya V, Christen B, Calzolai L, von Schroetter C, Fiorito F, Herrmann T, Güntert P, Wüthrich K (2005) Prion protein NMR structures of cats, dogs, pigs, and sheep. Proc Natl Acad Sci USA 102:640–645
43. Hawe A, Sutter M, Jiskoot W (2008) Extrinsic fluorescent dyes as tools for protein characterization. Pharm Res 25:1487–1499
44. Creighton TE (1990) Protein folding. Biochem J 270:1–16
45. Jahn TR, Parker MJ, Homans SW, Radford SE (2006) Amyloid formation under physiological conditions proceeds via a native-like folding intermediate. Nat Struct Mol Biol 13:195–201
46. Goldsbury C, Green J (2005) Time-lapse atomic force microscopy in the characterization of amyloid-like fibril assembly and oligomeric intermediates. Methods Mol Biol 299:103–128
47. Campioni S, Mossuto MF, Torrassa S, Calloni G, de Laureto PP, Relini A, Fontana A, Chiti F (2008) Conformational properties of the aggregation precursor state of HypF-N. J Mol Biol 379:554–567
48. Kaimann T, Metzger S, Kuhlmann K, Brandt B, Birkmann E, Höltje HD, Riesner D (2008) Molecular model of an alpha-helical prion protein dimer and its monomeric subunits as derived from chemical cross-linking and molecular modeling calculations. J Mol Biol 376:582–596
49. Kuwajima K (1989) The molten globule state as a clue for understanding the folding and cooperativity of globular-protein structure. Proteins 6:87–103
50. Sanz JM, Fersht AR (1993) Rationally designing the accumulation of a folding intermediate of barnase by protein engineering. Biochemistry 32:13584–13592
51. Pettersson-Kastberg J, Aits S, Gustafsson L, Mossberg A, Storm P, Trulsson M, Persson F, Mok KH, Svanborg C (2009) Can misfolded proteins be beneficial? The HAMLET case. Ann Med 41:162–176
52. Gambin Y, Schug A, Lemke EA, Lavinder JJ, Ferreon AC, Magliery TJ, Onuchic JN, Deniz AA (2009) Direct single-molecule observation of a protein living in two opposed native structures. Proc Natl Acad Sci USA 106:10153–10158
53. Silva JL, Vieira TC, Gomes MP, Bom AP, Lima LM, Freitas MS, Ishimaru D, Cordeiro Y, Foguel D (2009) Ligand binding and hydration in protein misfolding: insights from studies of prion and p53 tumor suppressor proteins (dagger). Acc Chem Res 43:271–279
54. Kremer W, Kachel N, Kuwata K, Akasaka K, Kalbitzer HR (2007) Species-specific differences in the intermediate states of human and Syrian hamster prion protein detected by high pressure NMR spectroscopy. J Biol Chem 282:22689–22698
55. Hou L, Kang I, Marchant RE, Zagorski MG (2002) Methionine 35 oxidation reduces fibril assembly of the amyloid abeta-(1–42) peptide of Alzheimer's disease. J Biol Chem 277:40173–40176
56. Bitan G, Tarus B, Vollers SS, Lashuel HA, Condron MM, Straub JE, Teplow DB (2003) A molecular switch in amyloid assembly: Met35 and amyloid beta-protein oligomerization. J Am Chem Soc 125:15359–15365
57. Requena JR, Dimitrova MN, Legname G, Teijeira S, Prusiner SB, Levine RL (2004) Oxidation of methionine residues in the prion protein by hydrogen peroxide. Arch Biochem Biophys 432:188–195
58. Breydo L, Bocharova OV, Makarava N, Salnikov VV, Anderson M, Baskakov IV (2005) Methionine oxidation interferes with conversion of the prion protein into the fibrillar proteinase K-resistant conformation. Biochemistry 44:15534–15543
59. Hart T, Hosszu LL, Trevitt CR, Jackson GS, Waltho JP, Collinge J, Clarke AR (2009) Folding kinetics of the human prion protein probed by temperature jump. Proc Natl Acad Sci USA 106:5651–5656
60. Lee S, Antony L, Hartmann R, Knaus KJ, Surewicz K, Surewicz WK, Yee VC (2010) Conformational diversity in prion protein variants influences intermolecular beta-sheet formation. EMBO J 29:251–262
61. Green KM, Browning SR, Seward TS, Jewell JE, Ross DL, Green MA, Williams ES, Hoover EA, Telling GC (2008) The elk PRNP codon 132 polymorphism controls cervid and scrapie prion propagation. J Gen Virol 89:598–608